

The reaction $\pi N \rightarrow \pi\pi N$ above threshold in chiral perturbation theory

V. Bernard¹, N. Kaiser², Ulf-G. Meißner³

¹*Laboratoire de Physique Théorique
Université Louis Pasteur, F-67037 Strasbourg Cedex 2, France
E-mail address: bernard@crnhp4.in2p3.fr*

²*Physik Department T39, TU München, D-85747 Garching, Germany
E-mail address: nkaiser@physik.tu-muenchen.de*

³*Institut für Kernphysik, Forschungszentrum Jülich, D-52425 Jülich, Germany
E-mail address: Ulf-G.Meissner@kfa-juelich.de*

Abstract

Single pion production off nucleons is studied in the framework of relativistic baryon chiral perturbation theory at tree level with the inclusion of the terms from the dimension two effective pion–nucleon Lagrangian. The five appearing low–energy constants are fixed from pion–nucleon scattering data. Despite the simplicity of the approach, most of the existing data for total and differential cross sections as well as for the angular correlation functions for incoming pion kinetic energies up to 400 MeV can be satisfactorily described.

1 Introduction

Single pion production off nucleons has been at the center of numerous experimental and theoretical investigations since many years. One of the original motivations of these works was the observation that the elusive pion–pion threshold S–wave interaction can be deduced from the pion–pole graph contribution. A whole series of precision experiments at PSI, TRIUMF and CERN has been performed over the last decade and there is still on–going activity. On the theoretical side, chiral perturbation theory has emerged as a precision tool in low energy hadron physics. Beringer considered the reaction $\pi N \rightarrow \pi\pi N$ to lowest order in chiral perturbation theory [1]. Low–energy theorems for the threshold amplitudes D_1 and D_2 ^{#1} were derived in [2]. These are free of unknown parameters and not sensitive to the $\pi\pi$ interaction beyond tree level. A direct comparison with the threshold data for the channel $\pi^+p \rightarrow \pi^+\pi^+n$, which is only sensitive to D_1 , lead to a very satisfactory description whereas in case of the process $\pi^-p \rightarrow \pi^0\pi^0n$, which is only sensitive to D_2 , sizeable deviations were found for the total cross sections near threshold. These were originally attributed to the strong pionic final–state interactions in the $I_{\pi\pi} = 0$ channel. However, this conjecture turned out to be incorrect when a complete higher order calculation of the threshold amplitudes $D_{1,2}$ was performed [3]. In that paper, we investigated the relation between the threshold amplitudes D_1 and D_2 for the reaction $\pi N \rightarrow \pi\pi N$ and the $\pi\pi$ S–wave scattering lengths a_0^0 and a_0^2 in the framework of heavy baryon chiral perturbation theory to second order in small momenta, i.e. the pion mass (which is the only small parameter at threshold). The pion loop and pionic counterterm corrections only start contributing to the $\pi\pi N$ threshold amplitudes at second order. One of these counterterms, proportional to the low–energy constant ℓ_3 , eventually allows to measure the scalar quark condensate, i.e. the strength of the spontaneous chiral symmetry breaking in QCD. However, at that order, the largest contribution stems indeed from insertions of the dimension two chiral pion–nucleon Lagrangian, which is characterized by a few coupling constants called c_i . In particular this is the case for the amplitude D_2 . To be specific, consider the threshold amplitudes $D_{1,2}$ calculated from the relativistic Born graphs (with lowest order vertices) and the relativistic c_i –terms expanded to second order in the pion mass. This gives

$$D_1^{\text{Born}} + D_1^{c_i} = (2.33 + 0.24 \pm 0.10) \text{ fm}^3 = (2.57 \pm 0.10) \text{ fm}^3, \quad (1)$$

$$D_2^{\text{Born}} + D_2^{c_i} = (-6.61 - 2.85 \pm 0.06) \text{ fm}^3 = (-9.46 \pm 0.06) \text{ fm}^3, \quad (2)$$

which are within 15% and 5% off the empirical values, $D_1^{\text{exp}} = (2.26 \pm 0.10) \text{ fm}^3$ and $D_2^{\text{exp}} = (-9.05 \pm 0.36) \text{ fm}^3$, respectively. It appears therefore natural to extend the same calculation above threshold and to compare to the large body of data for the various reaction channels that exist. It was already shown by Beringer [1] that taking simply the

^{#1}These are related to the more commonly used \mathcal{A}_{10} and \mathcal{A}_{32} by $\mathcal{A}_{32} = \sqrt{10}D_1$ and $\mathcal{A}_{10} = -2D_1 - 3D_2$.

relativistic Born terms does indeed not suffice to describe the total cross section data for incoming pion energies up to 400 MeV in most channels. Such a failure can be expected from the threshold expansion of D_2 , where the Born terms only amount to 75% of the empirical value. We therefore expect that the inclusion of the dimension two operators, which clearly improves the prediction for D_2 at threshold, will lead to a better description of the above threshold data. In particular, it will tell to which extent loop effects are necessary (and thus testing the sensitivity to the pion–pion interaction beyond tree level) and to which extent one has to incorporate resonance degrees of freedom like the Roper and the Δ –isobar as well as heavier mesons (σ, ρ, ω) as dynamical degrees of freedom (as it is done in many models, see e.g. [4] [5]). Our calculation is in spirit closest to the one of ref.[6], in which Beringer’s Born terms were supplemented by explicit Δ and Roper (tree) contributions. Clearly, the inclusion of the resonances as done in that paper is not based on a consistent power counting scheme but rather it is argued that phenomenology demands the extension of the effective Lagrangian to include these higher mass states. It will be of particular importance to directly compare our results to the ones presented there for the abovementioned reasons. Since we will only calculate tree level diagrams with at most one insertion from the dimension two pion–nucleon Lagrangian, it is advantageous to treat the nucleons as fully relativistic Dirac fields, since then one automatically generates all $1/m$ suppressed terms with fixed coefficients. Here, m denotes the nucleon mass. Only at next order, when loop graphs have to be included, the problems due to the additional large mass scale given by the nucleon mass appear [7]. Therefore, the calculation presented here can not easily be extended to higher orders in the chiral expansion. At this point, we stress that the amplitudes calculated from the tree graphs as done here are, of course, purely real. How severe this approximation is can only be judged when a full one loop calculation above threshold has been performed.

This paper is organized as follows. Section 2 contains some formal aspects including the definition of the T–matrix and of the pertinent observables. In section 3 we briefly review the effective Lagrangian underlying the calculation and discuss the tree level diagrams to be evaluated. Section 4 contains the results and discussions thereof. The appendices include more details about the kinematics, some lengthy formula appearing in the expressions for the observables and the explicit expressions for the invariant amplitudes.

2 Single pion production: Formal aspects

In this section, we outline the basic framework concerning the reaction $\pi N \rightarrow \pi\pi N$ above threshold. Some of the lengthy formulae are relegated to the appendices.

2.1 T-matrix and invariant amplitudes

We seek the T-matrix element for the process

$$\pi^a(k) + N(p_1) \rightarrow \pi^b(q_1) + \pi^c(q_2) + N(p_2) , \quad (3)$$

with N denoting a nucleon (neutron or proton) and π^a a pion of (cartesian) isospin a . This process is characterized by five independent Mandelstam variables,

$$s = (p_1 + k)^2, \quad s_1 = (q_1 + p_2)^2, \quad s_2 = (q_2 + p_2)^2, \quad t_1 = (q_1 - k)^2, \quad t_2 = (q_2 - k)^2. \quad (4)$$

All scalar products between the various momenta can be expressed in terms of these, see appendix A, and at threshold ($\vec{q}_1 = \vec{q}_2 = 0$, in the center-of-mass frame), we have

$$s^{\text{thr}} = (m + 2M_\pi)^2, \quad s_1^{\text{thr}} = s_2^{\text{thr}} = (m + M_\pi)^2, \quad t_1^{\text{thr}} = t_2^{\text{thr}} = -M_\pi^2 \frac{2m + M_\pi}{m + 2M_\pi}. \quad (5)$$

The $\pi N \rightarrow \pi\pi N$ transition matrix element can be expressed in terms of four invariant amplitudes, denoted $F_i(s, s_1, s_2, t_1, t_2)$ ($i = 1, 2, 3, 4$),

$$T = i \bar{u}_2 \gamma_5 [F_1 + (q_1 + q_2)F_2 + (q_1 - q_2)F_3 + (q_1 q_2 - q_2 q_1)F_4] u_1 . \quad (6)$$

with $u_{1,2}$ the Dirac spinor for the in- and outgoing nucleon, respectively. In the complete relativistic tree calculation to order q^2 , these are rational real functions of the five Mandelstam variables. The isospin decomposition of the invariant amplitudes reads (pulling out a common prefactor composed of coupling constants)

$$F_i = \frac{g_A}{8F_\pi^3} \left[\tau^a \delta^{bc} B_i^1 + (\tau^b \delta^{ac} + \tau^c \delta^{ab}) B_i^2 + (\tau^b \delta^{ac} - \tau^c \delta^{ab}) B_i^3 + i\epsilon^{abc} B_i^4 \right], \quad (7)$$

with g_A the nucleon axial-vector coupling constant and F_π the pion decay constant, respectively. The crossing properties of the isospin amplitudes can be readily deduced. Crossing the two out-going pion lines, $(q_1, b) \leftrightarrow (q_2, c)$, amounts to

$$B_i^j(s, s_1, s_2, t_1, t_2) = \epsilon_i \epsilon_j B_i^j(s, s_2, s_1, t_2, t_1), \quad \epsilon_{1,2} = +1, \quad \epsilon_{3,4} = -1. \quad (8)$$

In the physical reaction channels the relevant amplitudes are given by

$$\tilde{F}_i = \frac{g_A}{8F_\pi^3} \sum_{j=1}^4 \eta_j B_i^j, \quad (9)$$

with η_j channel dependent isospin factors. We calculate the amplitudes B_i^j in the isospin limit with the charged pion mass ($M_\pi = 139.57$ MeV) and the proton mass, $m =$

938.27 MeV, in order. Isospin breaking is done by shifting the kinetic energy of the incoming pion, T_π , from the isospin symmetric threshold

$$T_\pi^{\text{thr,iso}} = M_\pi \left(1 + \frac{3M_\pi}{2m} \right) = 170.71 \text{ MeV} \quad (10)$$

to the correct threshold. The pertinent isospin coefficients η_j and numerical values for this shift, called δT_π , for the five experimentally accessible reaction channels are

$$\pi^+ p \rightarrow \pi^+ \pi^+ n : \quad \eta_1 = 0, \eta_2 = 2\sqrt{2}, \eta_3 = 0, \eta_4 = 0, \delta T_\pi = +1.68 \text{ MeV} \quad (11)$$

$$\pi^+ p \rightarrow \pi^+ \pi^0 p : \quad \eta_1 = 0, \eta_2 = 1, \eta_3 = -1, \eta_4 = 1, \delta T_\pi = -5.95 \text{ MeV} \quad (12)$$

$$\pi^- p \rightarrow \pi^+ \pi^- n : \quad \eta_1 = \sqrt{2}, \eta_2 = \sqrt{2}, \eta_3 = \sqrt{2}, \eta_4 = 0, \delta T_\pi = +1.68 \text{ MeV} \quad (13)$$

$$\pi^- p \rightarrow \pi^0 \pi^0 n : \quad \eta_1 = \sqrt{2}, \eta_2 = 0, \eta_3 = 0, \eta_4 = 0, \delta T_\pi = -10.21 \text{ MeV} \quad (14)$$

$$\pi^- p \rightarrow \pi^0 \pi^- p : \quad \eta_1 = 0, \eta_2 = 1, \eta_3 = 1, \eta_4 = 1, \delta T_\pi = -5.95 \text{ MeV} . \quad (15)$$

2.2 Observables

The total cross section is a four-dimensional integral over a quadratic form in the amplitudes \tilde{F}_i ,

$$\sigma_{\text{tot}}(T_\pi) = \frac{\mathcal{S}}{(4\pi)^4 m \sqrt{T_\pi(T_\pi + 2M_\pi)}} \int \int_{z^2 < 1} d\omega_1 d\omega_2 \int_{-1}^1 dx_1 \int_0^\pi d\phi \sum_{i,j=1}^4 y_{ij} \tilde{F}_i^* \tilde{F}_j . \quad (16)$$

The weight functions y_{ij} are given in appendix A, and \mathcal{S} is a Bose symmetry factor, $\mathcal{S} = 1/2$ for identical pions in the final state and $\mathcal{S} = 1$ otherwise. The center-of-mass (CMS) kinematics is

$$s = (m + M_\pi)^2 + 2mT_\pi, \quad k_0 = \frac{s - m^2 + M_\pi^2}{2\sqrt{s}}, \quad |\vec{k}| = \sqrt{k_0^2 - M_\pi^2}, \quad |\vec{q}_i| = \sqrt{\omega_i^2 - M_\pi^2}, \quad (17)$$

$$s_i = s - 2\sqrt{s}\omega_{3-i} + M_\pi^2, \quad t_i = 2(M_\pi^2 - k_0\omega_i + |\vec{k}||\vec{q}_i|x_i) \quad (i = 1, 2), \quad (18)$$

$$x_2 = x_1 z + \sqrt{(1 - x_1^2)(1 - z^2)} \cos \phi, \quad (19)$$

$$z |\vec{q}_1| |\vec{q}_2| = \omega_1 \omega_2 - \sqrt{s}(\omega_1 + \omega_2) + M_\pi^2 + \frac{1}{2}(s - m^2). \quad (20)$$

Here, ϕ is the (auxiliary) angle between the planes spanned by \vec{q}_1 and \vec{k} as well as \vec{q}_1 and \vec{q}_2 . In accordance with the experimentalists convention, we have chosen the coordinate frame such that the incoming pion momentum \vec{k} defines the z -direction, whereas \vec{q}_1 , the momentum of π^b lies in the xz -plane. The polar angles θ_1 and θ_2 of the outgoing pions (with $x_i = \cos \theta_i$) are in general non-vanishing and so is the azimuthal angle ϕ_2 of π^c . By construction, the azimuthal angle of π^b is zero.

The double differential cross section in the CMS depends on T_π , ω_1 , and θ_1 . For this more exclusive quantity the energy ω_1 and the polar angle θ_1 of π^b are detected,

$$\frac{d^2\sigma}{d\omega_1 d\Omega_1} = \frac{2\mathcal{S}}{(4\pi)^5 \sqrt{s} |\vec{k}|} \int_{\omega_2^-}^{\omega_2^+} d\omega_2 \int_0^\pi d\phi \sum_{i,j=1}^4 y_{ij} \tilde{F}_i^* \tilde{F}_j \quad (21)$$

with the boundaries of the three-body phase space given by

$$\omega_2^\pm = \frac{1}{2(s - 2\sqrt{s}\omega_1 + M_\pi^2)} \left[(\sqrt{s} - \omega_1)(s - 2\sqrt{s}\omega_1 - m^2 + 2M_\pi^2) \pm |\vec{q}_1| \sqrt{(s - 2\sqrt{s}\omega_1 - m^2)^2 - 4m^2 M_\pi^2} \right]. \quad (22)$$

Also measured are triple differential cross sections. These depend on T_π , ω_1 , θ_1 , θ_2 , and ϕ_2 . The two angles of π^c are measured in addition, thus the three-particle final state is kinematically completely determined,

$$\frac{d^3\sigma}{d\omega_1 d\Omega_1 d\Omega_2} = \frac{|\vec{q}_1| |\vec{q}_2| \mathcal{S}}{(4\pi)^5 \sqrt{s} |\vec{k}| \tilde{E}_2} \sum_{i,j=1}^4 y_{ij} \tilde{F}_i^* \tilde{F}_j, \quad (23)$$

with s , s_1 , s_2 , t_1 , t_2 as before and

$$\tilde{E}_2 = E_2 \left(1 + \frac{\partial E_2}{\partial \omega_2} \right) = \frac{\omega_2 (\frac{1}{2}(s - m^2) - \sqrt{s}\omega_1) + M_\pi^2 (\omega_1 + \omega_2 - \sqrt{s})}{\omega_2^2 - M_\pi^2}, \quad (24)$$

with E_2 the final state nucleon energy. The cosine of the angle between \vec{q}_1 and \vec{q}_2 is given by

$$z = \cos \theta_1 \cos \theta_2 + \sin \theta_1 \sin \theta_2 \cos \phi_2, \quad (25)$$

and it is needed to express the energy of π^c as

$$\omega_2 = \frac{1}{2[(\sqrt{s} - \omega_1)^2 - z^2 |\vec{q}_1|^2]} \left\{ (\sqrt{s} - \omega_1)(s - 2\sqrt{s}\omega_1 - m^2 + 2M_\pi^2) - z |\vec{q}_1| \sqrt{(s - 2\sqrt{s}\omega_1 - m^2)^2 - 4M_\pi^2(m^2 + (1 - z^2) |\vec{q}_1|^2)} \right\}. \quad (26)$$

From the triple and double differential cross sections, one defines the angular correlation function W at fixed beam energy T_π ,

$$W(\omega_1, \theta_1, \theta_2, \phi_2) = 4\pi \frac{d^3\sigma}{d\omega_1 d\Omega_1 d\Omega_2} \Big/ \frac{d^2\sigma}{d\omega_1 d\Omega_1}. \quad (27)$$

This completes the necessary formalism for our calculation.

3 Calculation of the tree level amplitudes

In this section, we briefly discuss the effective chiral Lagrangian underlying our calculations. For more details we refer to the review [8] and to the paper [3]. We then show and discuss the various classes of tree diagrams contributing to the process $\pi N \rightarrow \pi\pi N$ to second order in the chiral expansion.

3.1 Effective Lagrangian

At low energies, the relevant degrees of freedom are hadrons, in particular the Goldstone bosons linked to the spontaneous chiral symmetry breaking. We consider here the two flavor case and thus deal with the triplet of pions, collected in the matrix $U(x) = u^2(x)$. It is straightforward to build an effective Lagrangian to describe their interactions, called $\mathcal{L}_{\pi\pi}$. This Lagrangian admits a dual expansion in small (external) momenta and quark (meson) masses as detailed below. Matter fields such as nucleons can also be included in the effective field theory based on the familiar notions of non-linearly realized chiral symmetry. The pertinent effective Lagrangian is called $\mathcal{L}_{\pi N}$, consisting of terms with exactly one nucleon in the initial and the final state. The various terms contributing to a process under consideration are organized according to their chiral dimension, which counts the number of derivatives and/or meson mass insertions. Here, we work to second order in the corresponding small parameter q (which is a generic symbol for an external momentum or pion mass). Consequently, the effective Lagrangian consists of the following pieces:

$$\mathcal{L}_{\text{eff}} = \mathcal{L}_{\pi\pi}^{(2)} + \mathcal{L}_{\pi N}^{(1)} + \mathcal{L}_{\pi N}^{(2)} , \quad (28)$$

where the index (i) gives the chiral dimension. The form of $\mathcal{L}_{\pi\pi}^{(2)} + \mathcal{L}_{\pi N}^{(1)}$ is standard. Let us discuss in some more detail the terms appearing in $\mathcal{L}_{\pi N}^{(2)}$. For the reasons outlined before, we treat the spin-1/2 fields, i.e. the nucleons, relativistically. The terms of the dimension two effective relativistic pion-nucleon Lagrangian relevant to our calculation read [7] [9]

$$\begin{aligned} \mathcal{L}_{\pi N}^{(2)} = & c_1 \bar{\Psi} \Psi \text{Tr}(\chi_+) + \frac{c'_2}{4m} \bar{\Psi} i \gamma_\mu \overleftrightarrow{D}_\nu \Psi \text{Tr}(u^\mu u^\nu) - \frac{c''_2}{8m^2} \bar{\Psi} \overleftrightarrow{D}_\mu \overleftrightarrow{D}_\nu \Psi \text{Tr}(u^\mu u^\nu) \\ & + c_3 \bar{\Psi} u_\mu u^\mu \Psi + c_4 \frac{i}{4} \bar{\Psi} \sigma_{\mu\nu} [u^\mu, u^\nu] \Psi , \end{aligned} \quad (29)$$

where Ψ denotes the relativistic nucleon field and with

$$\chi_+ = u^\dagger \chi u^\dagger + u \chi^\dagger u , \quad u_\mu = i u^\dagger \nabla_\mu U u^\dagger . \quad (30)$$

The quantity χ contains the light quark mass \hat{m} and external scalar and pseudoscalar sources [7] and ∇_μ is the standard chiral covariant derivative acting on the pion fields. The low-energy constants c_i are normalized such that we can identify them with the corresponding low-energy constants of the heavy baryon Lagrangian (truncated at order q^2) (for definitions, see e.g. [8]). Their numerical values have been determined in [3] from a tree level fit to pion-nucleon scattering (sub)threshold parameters,

$$\begin{aligned} c_1 &= -0.64 \pm 0.14 , & c'_2 &= -5.63 \pm 0.10 , & c''_2 &= 7.41 \pm 0.10 , \\ c_3 &= -3.90 \pm 0.09 , & c_4 &= 2.25 \pm 0.09 , \end{aligned} \quad (31)$$

with all numbers given in GeV^{-1} . It is important to stress that the effective Lagrangian we use does not incorporate any resonances like e.g. the $\Delta(1232)$ or the $N^*(1440)$ as

dynamical degrees of freedom. Their contribution is encoded in the numerical values of the low-energy constants c_i , for a more detailed discussion see [10]. Clearly, one might doubt that above threshold such a procedure is sufficient, since for example it does not account for the effects related to the widths of these resonances. If one expands the resonance propagators in powers of momentum transfer over resonance mass, one gets to leading order such dimension two pion-nucleon couplings as used here (plus an infinite series of higher order terms). Our study should therefore reveal at which kinematics and for which observables explicit resonance effects can be most easily seen. This would be helpful for pinning down various resonance couplings which are not too well constraint by the present models (when global fits are performed). Finally, we stress that the dimension two operators encode also information about t-channel meson exchanges, e.g. the constant c_1 is essentially saturated by scalar meson (correlated 2π , to be precise) exchange and c_4 receives an important contribution from the ρ [10].

3.2 Chiral expansion of the invariant amplitudes

Let \mathcal{B} be a generic symbol for any one of the B_i^j . The chiral expansion considered here takes the form

$$\mathcal{B} = \mathcal{B}^{\text{Born}} + \mathcal{B}^{c_i} \quad . \quad (32)$$

Consider first the Born terms with insertions solely from $\mathcal{L}_{\pi N}^{(1)}$ shown in Fig. 1. Diagram A involves the $NN3\pi$ -vertex genuine to $\pi N \rightarrow \pi\pi N$ at tree level. The lowest order four-pion interaction appears in the pion pole graph (B). The graphs of the classes C, D, E and F contain one pion-nucleon vertex and one Weinberg $NN\pi\pi$ interaction, thus these scale as g_A . The graphs belonging to the classes G, H and I each contain three pion-nucleon vertices and thus scale as g_A^3 . In Fig. 2, we show the term with exactly one insertion from $\mathcal{L}_{\pi N}^{(2)}$, i.e. these are proportional to the low-energy constants c_i . Note that there is no higher order $NN3\pi$ -vertex from the dimension two Lagrangian because of isospin. Note also that the graphs of type J, K, L and M are topologically identical to the ones of classes N, O, P and Q. However, while the operator proportional to c_4 contributes to the B_i^4 , the ones $\sim c_1, c'_2, c''_2$ and c_3 can not. The explicit formula for the B_i^j for the various (classes of) diagrams are given in appendix B.

4 Results and discussion

In this section, we show the results for the total and double differential cross sections as well as the angular correlation function in comparison to the available data. Our input parameters are $M_\pi = 139.57$ MeV, $m = 938.27$ MeV, $F_\pi = 92.4$ MeV and $g_A = 1.32$ as determined from the Goldberger-Treiman relation $g_A = F_\pi g_{\pi N}/m$ with $g_{\pi N} = 13.4$. For the low-energy constants c_i , we take the central values given in Eq.(31). Setting $c_i = 0$ corresponds to the tree level (dimension one) calculation of Beringer [1].

4.1 Total cross sections

First, we discuss the data from threshold up to incoming pion kinetic energy of $T_\pi = 400$ MeV and then take a closer look at the threshold regions, $T_\pi \leq 210$ MeV. In all graphs, the solid line gives the result with the c_i as given in Eq.(31) and the dashed line the one with the $c_i = 0$.

$\pi^+p \rightarrow \pi^+\pi^+n$, Fig. 3: The data are from refs. [11] [12] [13] [14]. The lowest order calculation does already quite well. Inclusion of the dimension two terms leads to a too large cross section. This can be traced back to the fact that the Born term result for the threshold amplitude D_1 is closer to the empirical number than the one with the c_i corrections, compare Eq.(1).

$\pi^+p \rightarrow \pi^+\pi^0p$, Fig. 4: There are recent data from [15] and a few older data in this kinematical range, see refs. [16] [17] [18]. While the lowest order calculation tends to underestimate the data above the threshold region, the c_i corrections lead to a somewhat too large total cross section, in particular when compared only to the data of [15].

$\pi^-p \rightarrow \pi^+\pi^-n$, Fig. 5: The data are from refs. [19] [20] [21] [22] [23] [24] [25] [26] [27]. The lowest order calculation clearly underestimate the cross section even close to threshold. Inclusion of the dimension two terms leads to an astonishingly good description of the total cross section up to $T_\pi = 400$ MeV.

$\pi^-p \rightarrow \pi^0\pi^0n$, Fig. 6: The data are from refs. [28] [29] [30] [31] [32]. The lowest order calculation clearly underestimates the cross section even close to threshold. Inclusion of the dimension two terms leads to a good description of the total cross section up to $T_\pi = 230$ MeV and a slight underestimation for larger pion energies.

$\pi^-p \rightarrow \pi^0\pi^-p$, Fig. 7: The data are from refs. [19] [21] [25]. Inclusion of the dimension two terms leads to an improved description of the total cross section up to $T_\pi = 250$ MeV and a slight overestimation for larger pion energies whereas the lowest order result is consistently below the data for $T_\pi > 230$ MeV.

Threshold region: The threshold regions for all five channels are shown in Figs. 8 and 9. In all but one case, i.e. for $\pi^+p \rightarrow \pi^+\pi^+n$, the inclusion of the terms $\sim c_i$ clearly improves the description of the data. As already noted in the introduction, this improvement is not due to the strong pionic rescattering in the isospin zero, S-wave as originally thought [2]. It should be noted, however, that only for $\pi^+p \rightarrow \pi^+\pi^+n$ and $\pi^-p \rightarrow \pi^0\pi^0n$, *precise* data close to threshold exist

4.2 Double differential cross sections

Double differential cross sections have been published by Manley [33] and by Müller et al. [34] for the reaction $\pi^-p \rightarrow \pi^+\pi^-n$. In Fig. 10, we show the results in comparison to the data of [33] at $\sqrt{s} = 1.242$ GeV and for $T_{\pi^+} = \omega_1 - M_\pi = 6.5, 10.95$ and 15.35 MeV, in order. Fig. 11 comprises the results for $\sqrt{s} = 1.262$ GeV and $T_{\pi^+} = \omega_1 - M_\pi = 10.4, 17.5$ and 24.6 MeV. In all cases, our full calculation describes well the data whereas the leading

order calculation is systematically below these. However, we are not able to describe the data of [34] at $\sqrt{s} = 1.301$ GeV as shown in Fig. 12. The two solid lines in that figure refer to the angular range of $x_1 = \cos \theta_1$, $0.03 < x_1 < 0.35$. The strong peaking of the data around $T_{\pi^+} = \omega_1 - M_\pi \simeq 25$ MeV can not be reproduced. Two comments are in order. The experiment of [34] was not intended primarily to measure the double differential cross section but rather the angular correlation function, see the next paragraph. It is, however, claimed in [34] that their results for $d^2\sigma/d\omega_1 d\Omega_1$ agree with the ones of Manley [33] [35] once a scaling factor to account for the different incident pion kinetic energies is applied and the different laboratory angles of both experiments are considered. Other double differential cross sections for the same process measured by the Erlangen group are given in [36] [37]. These span the range of the incoming pion kinetic energy T_{π^-} from 218 to 330 MeV. The data for the lower energies are well described within our approach, as shown in Fig. 13. For beam energies $T_{\pi^-} = 246$ and 330 MeV, our results underestimate the data, but not as strongly as for the data of [34] at $T_{\pi^-} = 284$ MeV.

4.3 Angular correlation functions

An extensive study of the angular correlation function W for $\pi^- p \rightarrow \pi^+ \pi^- n$ at $\sqrt{s} = 1.301$ GeV is given in [34]. For six values of the momentum of the positive pion, $|\vec{q}_1| = 60.5, 86, 100, 113, 127$ and 151.5 MeV^{#2} tables are given for W as a function of ϕ_2 (with θ_2 fixed) and of θ_2 (with ϕ_2 fixed). We scanned through all of these data and found the following results. For fixed θ_2 , the angular correlation function is well described as long as $\phi_2 > 50^\circ$. For smaller azimuthal angles, we consistently underestimate the data, a typical example is shown in Fig. 14. On the other hand, for the fixed values of ϕ_2 given in [34], the θ_2 dependence is satisfactorily described, two examples are given in Fig. 15. We have also considered the angular correlation functions given in [36] and [37] and found similar trends, i.e. in general a good description of W as long as the dimension two terms are taken into account.

4.4 Comparison to other calculations

As already stated, the calculation of [6] is in spirit closest to ours. They use the relativistic pion–nucleon Lagrangian to leading order^{#3} and add explicit Δ and Roper degrees of freedom, but no heavy meson (σ , ρ) exchanges. Overall, their results are not significantly better than ours. It is important to note that these authors did not try a best fit by fine tuning the various coupling constants. Our conclusion is similar to theirs, namely that for really testing the constraints from chiral symmetry, one needs more precise data at low energies. The model of [4] is more elaborate concerning the inclusion of meson exchanges

^{#2}We use the central values of the pertinent momentum bins.

^{#3}They are not using heavy baryon CHPT as claimed in their paper.

and is more tuned to the resonance than to the threshold region. Similarly, the work of the Erlangen group [5] shows the importance of the non-linear pion couplings at tree level but does not include higher derivative operators as done here. Our approach lends more credit to the conclusions of these papers that the intricate dynamics of the reaction $\pi N \rightarrow \pi\pi N$ reveals itself best in double differential cross sections and angular correlation functions but not in the total cross sections.

5 Summary and conclusions

In this paper, we have studied the reaction $\pi N \rightarrow \pi\pi N$ in relativistic baryon chiral perturbation theory at tree level including the dimension two pion-nucleon Lagrangian. This study was motivated by the fact that at threshold the dominant corrections to the lowest order tree graphs indeed come from tree graphs with exactly one insertion from $\mathcal{L}_{\pi N}^{(2)}$ and not from loop graphs, as shown in [3]. The values of the relevant low-energy constants can be fixed from a few pion-nucleon scattering data. These low-energy constants encode information about baryonic and mesonic resonance excitations, in particular related to the Δ , the Roper, the ρ and the correlated two-pion exchange in the scalar-isoscalar channel [10]. Consequently, all our results concerning single pion production are based on a truly parameter-free calculation. The pertinent results of this study can be summarized as follows:

- For pion energies up to $T_\pi = 250$ MeV, in all but one case the inclusion of the contribution $\sim c_i$ clearly improves the description of the total cross sections, most notably in the threshold region for $\pi^- p \rightarrow \pi^0 \pi^0 n$. Up to $T_\pi = 400$, the trend of the data can be described although some discrepancies particularly towards the higher energies persist, see Figs. 3..9. This indicates that our approach is best suited for the threshold regions.
- Double differential cross sections for $\pi^- p \rightarrow \pi^+ \pi^- n$ at incident pion energies below $T_\pi = 250$ MeV are well described (see Figs. 10,11,13). We are not able to reproduce the strong peak of $d^2\sigma/d\omega_1 d\Omega_1$ as a function the outgoing π^+ energy at $\sqrt{s} = 1.301$ GeV found in [34], compare Fig. 12.
- The angular correlation function for the reaction $\pi^- p \rightarrow \pi^+ \pi^- n$ as given in [34] can be reproduced fairly well for all energy bins and sets of polar and azimuthal angles given in that paper, with the exception of small polar angles for the final-state negative pion, compare Figs. 14 and 15.

Acknowledgements

We thank W. Eyrich and M. Moosburger for valuable information on the experimental data.

A Kinematics and weight functions

First, we express all possible scalar products of the nucleon and pion momenta in the initial and final state in terms of the five Mandelstam invariants, see Eq.(4), and the particle masses,

$$2p_1 \cdot k = s - m^2 - M_\pi^2, \quad 2p_1 \cdot q_1 = s - s_2 + t_1 - M_\pi^2, \quad 2p_1 \cdot q_2 = s - s_1 + t_2 - M_\pi^2, \quad (\text{A.1})$$

$$2p_1 \cdot p_2 = s_1 + s_2 - s - t_1 - t_2 + m^2 + M_\pi^2, \quad 2k \cdot q_1 = 2M_\pi^2 - t_1, \quad 2k \cdot q_2 = 2M_\pi^2 - t_2, \quad (\text{A.2})$$

$$2k \cdot p_2 = s + t_1 + t_2 - m^2 - 3M_\pi^2, \quad 2q_1 \cdot q_2 = s - s_1 - s_2 + m^2, \quad (\text{A.3})$$

$$2q_1 \cdot p_2 = s_1 - m^2 - M_\pi^2, \quad 2q_2 \cdot p_2 = s_2 - m^2 - M_\pi^2. \quad (\text{A.4})$$

The weight functions y_{ij} appearing in Eqs.(16,21,23) are given by:

$$\begin{aligned} y_{11} &= s_1 + s_2 - t_1 - t_2 - s - m^2 + M_\pi^2, \\ y_{12} &= m(2(s_1 + s_2 - s - m^2) - t_1 - t_2), \\ y_{13} &= m(t_2 - t_1), \\ y_{14} &= (s_1 - s_2)(s - s_1 - s_2 + m^2) + (t_1 - t_2)(m^2 + M_\pi^2) + s_1 t_2 - s_2 t_1, \\ y_{22} &= (s_1 + s_2)(4m^2 - M_\pi^2) + (t_1 + t_2)(s - m^2) + s^2 - 3s(2m^2 + M_\pi^2) \\ &\quad - 3m^2(m^2 + M_\pi^2) + 2M_\pi^4, \\ y_{23} &= (s_1 - s_2)(s - m^2 - 2M_\pi^2) + (t_2 - t_1)(m^2 + M_\pi^2) + s_1 t_1 - s_2 t_2, \\ y_{24} &= m(2s_1 - 2s_2 + t_1 - t_2)(s - s_1 - s_2 + m^2 + 2M_\pi^2), \\ y_{33} &= (s_1 + s_2)(2s - 2m^2 - 3M_\pi^2) + (t_1 + t_2)(2M_\pi^2 - m^2 - s) - 4s_1 s_2 \\ &\quad + 2s_1 t_1 + 2s_2 t_2 - s^2 + s(2m^2 + 3M_\pi^2) + 3m^4 - 5m^2 M_\pi^2 - 2M_\pi^4, \\ y_{34} &= m(2s + t_1 + t_2 - 2m^2 - 4M_\pi^2)(s - s_1 - s_2 + m^2 - 2M_\pi^2), \\ y_{44} &= (s - s_1 - s_2 + m^2)[(s - m^2)(s + t_1 + t_2 - m^2) + (s_1 - s_2)(s_2 - s_1 + t_2 - t_1)] \\ &\quad + M_\pi^2\{4M_\pi^2(2s - M_\pi^2) + m^2[3m^2 - 8M_\pi^2 + 6(s - s_1 - s_2) + 2(t_1 + t_2)] \\ &\quad - 5s^2 + 2s(s_1 + s_2 - t_1 - t_2) - s_1^2 - s_2^2 + 6s_1 s_2 + 2(s_1 - s_2)(t_2 - t_1)\}. \end{aligned} \quad (\text{A.5})$$

and they are symmetric under interchange of the indices, $y_{ij} = y_{ji}$.

B Invariant amplitudes B_i^j

In this appendix we give the invariant amplitudes B_i^j for individual (classes of) diagrams. The B_i^j not specified are zero for the class of diagrams just considered. The following abbreviations for kinematical quantities are used:

$$d_1 = s_1 - m^2, \quad d_2 = s_2 - m^2, \quad d_3 = 2M_\pi^2 - s + s_1 - t_2, \quad (\text{B.1})$$

$$d_4 = 2M_\pi^2 - s + s_2 - t_1, \quad d_5 = m^2 + 4M_\pi^2 - s - t_1 - t_2, \quad d_6 = s - m^2. \quad (\text{B.2})$$

Diagram A:

$$B_2^1 = 2, \quad B_1^2 = 4m, \quad B_2^2 = B_3^3 = -1. \quad (\text{B.3})$$

Diagram B:

$$B_1^1 = \frac{8m(d_1 + d_2 - d_6 - M_\pi^2)}{2M_\pi^2 - d_1 - d_2 - d_5}, \quad B_1^2 = \frac{4m(2M_\pi^2 - t_1 - t_2)}{2M_\pi^2 - d_1 - d_2 - d_5}, \quad B_1^3 = \frac{4m(t_1 - t_2)}{2M_\pi^2 - d_1 - d_2 - d_5}. \quad (\text{B.4})$$

Here, the separation of the invariant amplitudes between diagram A and B results from using the σ -model gauge, $U = \sqrt{1 - \vec{\pi}^2/F_\pi^2} + i\vec{\tau} \cdot \vec{\pi}/F_\pi$. We have checked that other parametrizations lead to the same result for diagram A plus B.

Diagram C:

$$B_1^3 = B_1^4 = 2m(s_2 - s_1)d_6^{-1}, \quad B_3^3 = B_3^4 = 1, \quad B_4^3 = B_4^4 = -2md_6^{-1}. \quad (\text{B.5})$$

Diagram D:

$$B_1^3 = -B_1^4 = 2m(d_3 - d_4)d_5^{-1}, \quad B_3^3 = -B_3^4 = 1, \quad B_4^3 = -B_4^4 = 2md_5^{-1}. \quad (\text{B.6})$$

Diagrams E:

$$B_1^1 = -2B_1^2 = 2m(d_1 + d_2 - d_6)(d_1^{-1} + d_2^{-1}), \quad B_2^1 = -2B_2^2 = -3, \quad (\text{B.7})$$

$$B_4^1 = -2B_4^2 = 2m(d_2^{-1} - d_1^{-1}), \quad B_1^4 = 2B_1^3 = 2m(d_1 + d_2 - d_6)(d_1^{-1} - d_2^{-1}), \quad (\text{B.8})$$

$$B_3^4 = 2B_3^3 = 1, \quad B_4^4 = 2B_4^3 = -2m(d_1^{-1} + d_2^{-1}). \quad (\text{B.9})$$

Diagrams F:

$$B_1^1 = -2B_1^2 = 2m(d_1 + d_2 - d_6)(d_3^{-1} + d_4^{-1}), \quad B_2^1 = -2B_2^2 = -3, \quad (\text{B.10})$$

$$B_4^1 = -2B_4^2 = 2m(d_4^{-1} - d_3^{-1}), \quad B_1^4 = -2B_1^3 = 2m(d_1 + d_2 - d_6)(d_3^{-1} - d_4^{-1}), \quad (\text{B.11})$$

$$B_3^4 = -2B_3^3 = -1, \quad B_4^4 = -2B_4^3 = -2m(d_3^{-1} + d_4^{-1}). \quad (\text{B.12})$$

Diagrams G:

$$B_1^1 = g_A^2 m d_6^{-1} \{ (s + 3m^2) [(s - s_1)d_2^{-1} + (s - s_2)d_1^{-1}] - 4(s + m^2) \}, \quad (\text{B.13})$$

$$B_1^3 = B_1^4 = g_A^2 m d_6^{-1} \{ (s + 3m^2) [(s - s_2)d_1^{-1} - (s - s_1)d_2^{-1}] + 2(s_1 - s_2) \}, \quad (\text{B.14})$$

$$B_2^1 = g_A^2 [8m^2 d_6^{-1} + 1 - 2m^2(d_1^{-1} + d_2^{-1})], \quad B_2^3 = B_2^4 = B_3^1 = 2g_A^2 m^2 (d_2^{-1} - d_1^{-1}), \quad (\text{B.15})$$

$$B_3^3 = B_3^4 = g_A^2 [-1 - 2m^2(d_1^{-1} + d_2^{-1})], \quad B_4^1 = g_A^2 m (s + 3m^2) d_6^{-1} (d_1^{-1} - d_2^{-1}), \quad (\text{B.16})$$

$$B_4^3 = B_4^4 = g_A^2 m d_6^{-1} [2 + (s + 3m^2)(d_1^{-1} + d_2^{-1})]. \quad (\text{B.17})$$

Diagrams H:

$$B_1^1 = -B_1^2 = g_A^2 m \{ 2 + (s - s_2) d_1^{-1} + (s - s_1) d_2^{-1} \\ + (d_6 - d_1 - d_2) [(3m^2 + s_1) d_1^{-1} d_3^{-1} + (3m^2 + s_2) d_2^{-1} d_4^{-1}] \}, \quad (\text{B.18})$$

$$B_1^4 = g_A^2 m \{ (s - s_2) d_1^{-1} - (s - s_1) d_2^{-1} + (d_6 - d_1 - d_2) [(3m^2 + s_1) d_1^{-1} d_3^{-1} - (3m^2 + s_2) d_2^{-1} d_4^{-1}] \}, \quad (\text{B.19})$$

$$B_2^1 = -B_2^2 = 2g_A^2 [1 + m^2 (d_1^{-1} + d_2^{-1} + d_3^{-1} + d_4^{-1})], \quad B_2^4 = 2g_A^2 m^2 (d_1^{-1} - d_2^{-1} + d_3^{-1} - d_4^{-1}), \quad (\text{B.20})$$

$$B_3^1 = -B_3^2 = 2g_A^2 m^2 (d_1^{-1} - d_2^{-1} - d_3^{-1} + d_4^{-1}), \quad (\text{B.21})$$

$$B_3^4 = 2g_A^2 m^2 (d_1^{-1} + d_2^{-1} - d_3^{-1} - d_4^{-1}), \quad (\text{B.22})$$

$$B_4^1 = -B_4^2 = g_A^2 m [(4m^2 + d_1 + d_3) d_1^{-1} d_3^{-1} - (4m^2 + d_2 + d_4) d_2^{-1} d_4^{-1}], \quad (\text{B.23})$$

$$B_4^4 = g_A^2 m [(4m^2 + d_1 + d_3) d_1^{-1} d_3^{-1} + (4m^2 + d_2 + d_4) d_2^{-1} d_4^{-1}]. \quad (\text{B.24})$$

Diagrams I:

$$B_1^1 = g_A^2 m d_5^{-1} \{ (4m^2 + d_5) [(d_5 - d_4) d_3^{-1} + (d_5 - d_3) d_4^{-1}] - 4(d_5 + 2m^2) \}, \quad (\text{B.25})$$

$$B_1^3 = -B_1^4 = g_A^2 m d_5^{-1} \{ (d_5 + 4m^2) [(d_5 - d_3) d_4^{-1} - (d_5 - d_4) d_3^{-1}] + 2(d_4 - d_3) \}, \quad (\text{B.26})$$

$$B_2^1 = g_A^2 [1 + 8m^2 d_5^{-1} - 2m^2 (d_3^{-1} + d_4^{-1})], \quad B_2^3 = -B_2^4 = B_3^1 = 2g_A^2 m^2 (d_3^{-1} - d_4^{-1}), \quad (\text{B.27})$$

$$B_3^3 = -B_3^4 = g_A^2 [-1 - 2m^2 (d_3^{-1} + d_4^{-1})], \quad B_4^1 = g_A^2 m (d_5 + 4m^2) d_5^{-1} (d_3^{-1} - d_4^{-1}), \quad (\text{B.28})$$

$$B_4^3 = -B_4^4 = g_A^2 m d_5^{-1} [-2 - (d_5 + 4m^2) (d_3^{-1} + d_4^{-1})]. \quad (\text{B.29})$$

Diagrams J:

$$B_1^1 = d_6^{-1} \{ 4(3m^2 + s) [4c_1 M_\pi^2 + c_3 (d_6 - d_2 - d_1)] + [d_6^2 - (d_1 - d_2)^2] (2c_2' + c_2'' (d_6 / (2m^2) + 2)) \}, \quad (\text{B.30})$$

$$B_2^1 = -d_6 (c_2' + c_2'') / m - m d_6^{-1} [32c_1 M_\pi^2 - c_2'' (d_1 - d_2)^2 / m^2 + 8c_3 (d_6 - d_2 - d_1)], \quad (\text{B.31})$$

$$B_3^1 = c_2' (s_1 - s_2) / m, \quad B_4^1 = 2c_2' (s_2 - s_1) d_6^{-1}. \quad (\text{B.32})$$

Diagrams K:

$$B_1^1 = d_5^{-1} \{ 4(4m^2 + d_5) [4c_1 M_\pi^2 + c_3 (d_6 - d_2 - d_1)] + [d_5^2 - (d_3 - d_4)^2] (2c_2' + c_2'' (d_5 / (2m^2) + 2)) \}, \quad (\text{B.33})$$

$$B_2^1 = -d_5 (c_2' + c_2'') / m - m d_5^{-1} [32c_1 M_\pi^2 - c_2'' (d_3 - d_4)^2 / m^2 + 8c_3 (d_6 - d_2 - d_1)], \quad (\text{B.34})$$

$$B_3^1 = c_2' (d_4 - d_3) / m, \quad B_4^1 = 2c_2' (d_4 - d_3) d_5^{-1}. \quad (\text{B.35})$$

Diagrams L:

$$B_1^2 = 16c_1 M_\pi^2 - 2c_3 (d_5 + d_6) + c_2' (d_6 - d_1 - d_2) [(d_3 - d_6) d_1^{-1} + (d_4 - d_6) d_2^{-1}] \\ + c_2'' / (2m^2) [(d_6 - M_\pi^2 + t_1 / 2) (d_4 - s + s_2) + (d_6 - M_\pi^2 + t_2 / 2) (d_3 - s + s_1)], \quad (\text{B.36})$$

$$\begin{aligned}
B_1^3 &= 2c_3(t_2 - t_1) + c'_2(d_6 - d_1 - d_2)\{[2(M_\pi^2 - d_6) - t_2]d_1^{-1} - [2(M_\pi^2 - d_6) - t_1]d_2^{-1}\} \\
&\quad + c''_2/m^2[m^2(s_2 - s_1 + (t_2 - t_1)/2) + (s - M_\pi^2)(d_3 - d_4) \\
&\quad + t_2/2(s_1 - t_2/2) - t_1/2(s_2 - t_1/2)], \tag{B.37}
\end{aligned}$$

$$\begin{aligned}
B_2^2 &= 8c_1M_\pi^2m(d_1^{-1} + d_2^{-1}) + 2c_3m[(t_2 - 2M_\pi^2)d_1^{-1} + (t_1 - 2M_\pi^2)d_2^{-1}] \\
&\quad + c'_2/m[m^2 + 3M_\pi^2 - 3s + s_1 + s_2 - 3/4(t_1 + t_2)] + c''_2/m[2(d_6 - M_\pi^2) \\
&\quad + (t_1 + t_2)/2 - (s + t_2/2 - m^2 - M_\pi^2)^2d_1^{-1} - (s + t_1/2 - m^2 - M_\pi^2)^2d_2^{-1}], \tag{B.38}
\end{aligned}$$

$$\begin{aligned}
B_2^3 &= 8c_1M_\pi^2m(d_1^{-1} - d_2^{-1}) + 2c_3m[(t_2 - 2M_\pi^2)d_1^{-1} - (t_1 - 2M_\pi^2)d_2^{-1}] \\
&\quad + c'_2/m[s_1 - s_2 + 3/4(t_1 - t_2)] + c''_2/m[(t_2 - t_1)/2 \\
&\quad - (s + t_2/2 - m^2 - M_\pi^2)^2d_1^{-1} + (s + t_1/2 - m^2 - M_\pi^2)^2d_2^{-1}], \tag{B.39}
\end{aligned}$$

$$B_3^2 = B_2^3 + c'_2(d_4 - d_3)/m, \tag{B.40}$$

$$B_3^3 = B_2^2 + c'_2(3s - m^2 - s_1 - s_2 - d_5)/m, \tag{B.41}$$

$$B_4^2 = c'_2[(2(M_\pi^2 - d_6) - t_2)d_1^{-1} - (2(M_\pi^2 - d_6) - t_1)d_2^{-1}], \tag{B.42}$$

$$B_4^3 = c'_2[2 + (2(M_\pi^2 - d_6) - t_2)d_1^{-1} + (2(M_\pi^2 - d_6) - t_1)d_2^{-1}]. \tag{B.43}$$

Diagrams M:

$$\begin{aligned}
B_1^2 &= 16c_1M_\pi^2 - 2c_3(d_5 + d_6) + c'_2(d_6 - d_1 - d_2)[(d_1 - d_5)d_3^{-1} + (d_2 - d_5)d_4^{-1}] \\
&\quad + c''_2/m^2[(d_6 - 3M_\pi^2 + t_1/2 + t_2)(M_\pi^2 - d_1 - t_1/2) \\
&\quad + (d_6 - 3M_\pi^2 + t_2/2 + t_1)(M_\pi^2 - d_2 - t_2/2)], \tag{B.44}
\end{aligned}$$

$$\begin{aligned}
B_1^3 &= 2c_3(t_2 - t_1) + c'_2(d_6 - d_1 - d_2)\{[(d_2 - d_5)d_4^{-1} - (d_1 - d_5)d_3^{-1}] \\
&\quad + c''_2/m^2[(d_6 - 3M_\pi^2)(s_1 - s_2) + (t_1 - t_2)(s/2 - M_\pi^2) \\
&\quad + (t_1/2 + t_2)(t_1/2 + s_1) - (t_2/2 + t_1)(t_2/2 + s_2)], \tag{B.45}
\end{aligned}$$

$$\begin{aligned}
B_2^2 &= 8c_1M_\pi^2m(d_3^{-1} + d_4^{-1}) + 2c_3m[(t_2 - 2M_\pi^2)d_4^{-1} + (t_1 - 2M_\pi^2)d_3^{-1}] \\
&\quad + c'_2/m[s - 3m^2 - 5M_\pi^2 + s_1 + s_2 + 5/4(t_1 + t_2)] + c''_2/m[d_1 + d_2 + (t_1 + t_2)/2 \\
&\quad - 2M_\pi^2 - (s_1 + t_1/2 - m^2 - M_\pi^2)^2d_3^{-1} - (s_2 + t_2/2 - m^2 - M_\pi^2)^2d_4^{-1}], \tag{B.46}
\end{aligned}$$

$$\begin{aligned}
B_2^3 &= 8c_1M_\pi^2m(d_4^{-1} - d_3^{-1}) + 2c_3m[(t_2 - 2M_\pi^2)d_4^{-1} - (t_1 - 2M_\pi^2)d_3^{-1}] \\
&\quad + c'_2/m[s_2 - s_1 + (t_2 - t_1)/4] + c''_2/m[s_2 - s_1 + (t_2 - t_1)/2 \\
&\quad + (s_1 + t_1/2 - m^2 - M_\pi^2)^2d_3^{-1} - (s_2 + t_2/2 - m^2 - M_\pi^2)^2d_4^{-1}], \tag{B.47}
\end{aligned}$$

$$B_3^2 = B_2^3 + c_2'(s_1 - s_2)/m, \quad (\text{B.48})$$

$$B_3^3 = B_2^2 + c_2'(2d_5 - d_1 - d_2), \quad (\text{B.49})$$

$$B_4^2 = c_2'[(2(d_1 - M_\pi^2) + t_1)d_3^{-1} - (2(d_2 - M_\pi^2) + t_2)d_4^{-1}], \quad (\text{B.50})$$

$$B_4^3 = c_2'[2 - (2(d_1 - M_\pi^2) + t_1)d_3^{-1} - (2(d_2 - M_\pi^2) + t_2)d_4^{-1}]. \quad (\text{B.51})$$

Diagram N:

$$B_2^3 = B_2^4 = 4c_4m(s_2 - s_1)d_6^{-1}, \quad B_3^3 = B_3^4 = 4c_4m, \quad B_4^3 = B_4^4 = -2c_4(s + 3m^2)d_6^{-1}. \quad (\text{B.52})$$

Diagram O:

$$B_2^3 = -B_2^4 = 4c_4m(d_3 - d_4)d_5^{-1}, \quad B_3^3 = -B_3^4 = 4c_4m, \quad B_4^3 = -B_4^4 = 2c_4(d_5 + 4m^2)d_5^{-1}. \quad (\text{B.53})$$

Diagram P:

$$B_1^1 = -2B_1^2 = 2c_4\{s + 7m^2 - d_5 + 4m^2[(s_2 - s)d_1^{-1} + (s_1 - s)d_2^{-1}]\}, \quad (\text{B.54})$$

$$B_1^4 = 2B_1^3 = 2c_4\{2(s_2 - s_1) + t_2 - t_1 + 4m^2[(s_2 - s)d_1^{-1} - (s_1 - s)d_2^{-1}]\}, \quad (\text{B.55})$$

$$B_2^1 = -2B_2^2 = 2c_4m[-8 + (2(d_6 - M_\pi^2) + t_2)d_1^{-1} + (2(d_6 - M_\pi^2) + t_1)d_2^{-1}], \quad (\text{B.56})$$

$$B_2^4 = 2B_2^3 = 2c_4m[(2(d_6 - M_\pi^2) + t_2)d_1^{-1} - (2(d_6 - M_\pi^2) + t_1)d_2^{-1}], \quad (\text{B.57})$$

$$B_3^1 = -2B_3^2 = B_2^4, \quad B_3^4 = 2B_3^3 = B_2^1 + 16c_4m, \quad (\text{B.58})$$

$$B_4^1 = -2B_4^2 = 8c_4m^2(d_2^{-1} - d_1^{-1}), \quad B_4^4 = 2B_4^3 = -4c_4[1 + 2m^2(d_1^{-1} + d_2^{-1})]. \quad (\text{B.59})$$

Diagram Q:

$$B_1^1 = -2B_1^2 = 2c_4[d_5 - d_6 + 4m^2(d_1 + d_2 - d_6)(d_3^{-1} + d_4^{-1})], \quad (\text{B.60})$$

$$B_1^4 = -2B_1^3 = 2c_4[2(s_2 - s_1) + t_2 - t_1 + 4m^2(d_1 + d_2 - d_6)(d_3^{-1} - d_4^{-1})], \quad (\text{B.61})$$

$$B_2^1 = -2B_2^2 = 4c_4m[-4 + (m^2 + 3M_\pi^2 - s - t_2 - t_1/2)d_3^{-1} + (m^2 + 3M_\pi^2 - s - t_1 - t_2/2)d_4^{-1}], \quad (\text{B.62})$$

$$B_2^4 = -2B_2^3 = 4c_4m[(m^2 + 3M_\pi^2 - s - t_2 - t_1/2)d_3^{-1} - (m^2 + 3M_\pi^2 - s - t_1 - t_2/2)d_4^{-1}], \quad (\text{B.63})$$

$$B_3^1 = -2B_3^2 = -B_2^4, \quad B_3^4 = -2B_3^3 = -B_2^1 - 16c_4m, \quad (\text{B.64})$$

$$B_4^1 = -2B_4^2 = 8c_4m^2(d_4^{-1} - d_3^{-1}), \quad B_4^4 = -2B_4^3 = -4c_4[1 + 2m^2(d_3^{-1} + d_4^{-1})]. \quad (\text{B.65})$$

References

- [1] J. Beringer, πN Newsletter 7 (1992) 33.
- [2] V. Bernard, N. Kaiser and Ulf-G. Meißner, Phys. Lett. B332 (1994) 415; (E) B338 (1994) 520.
- [3] V. Bernard, N. Kaiser, and Ulf-G. Meißner, Nucl. Phys. B457 (1995) 147.
- [4] E. Oset and M.J. Vicente-Vacas, Nucl. Phys. A446 (1985) 584.
- [5] O. Jäkel, H.W. Ortner, M. Dillig and C.A.Z. Vasconcellos, Nucl. Phys. A511 (1990) 733; O. Jäkel, M. Dillig and C.A.Z. Vasconcellos, Nucl. Phys. A541 (1992) 675.
- [6] T.S. Jensen and A. Miranda, πN Newsletter 10 (1995) 179; T.S. Jensen and A. Miranda, Phys. Rev. C (1997) in print
- [7] J. Gasser, M.E. Sainio and A. Švarc, Nucl. Phys. B307 (1988) 779.
- [8] V. Bernard, N. Kaiser, and Ulf-G. Meißner, Int. J. Mod. Phys. E4 (1995) 193.
- [9] A. Krause, Helv. Acta Phys. 63 (1990) 3.
- [10] V. Bernard, N. Kaiser, and Ulf-G. Meißner, [hep-ph/9611253], Nucl. Phys. A, in print.
- [11] M. Sevier et al., Phys. Rev. Lett. 66 (1991) 2569
- [12] G. Kernel et al., Z. Phys. C48 (1990) 201.
- [13] A.V. Kratsov et al., Leningrad Institute of Nuclear Physics preprint No. 209, 1976.
- [14] J. Kirz, J. Schwartz and R.D. Tripp, Phys. Rev. 126 (1962) 763.
- [15] D. Počanić et al., Phys. Rev. Lett. 72 (1993) 1156.
- [16] Yu.A. Batsuov et al., Sov. J. Nucl. Phys. 21 (1975) 162.
- [17] M. Arman et al., Phys. Rev. Lett. 29 (1972) 962.
- [18] V. Barnes et al., CERN Report 63-27, 1963.
- [19] G. Kernel et al., Phys. Lett. B216 (1989) 244; *ibid* B225 (1989) 198.
- [20] C.W. Bjork et al., Phys. Rev. Lett. 44 (1980) 62.
- [21] J.A. Jones, W.W.M. Allison and D.H. Saxon, Nucl. Phys. B83 (1974) 93.
- [22] I.M. Blair et al., Phys. Lett. B32 (1970) 528.
- [23] D.H. Saxon, J.H. Mulvey and W. Chinowsky, Phys. Rev. D2 (1970) 1790.
- [24] Yu.A. Batsuov et al., Sov. J. Nucl. Phys. 1 (1965) 374.

- [25] T.D. Blokhintseva et al., Sov. Phys. JETP 17 (1963) 340.
- [26] J. Deahl et al., Phys. Rev. 124 (1961) 1987.
- [27] W.A. Perkins et al., Phys. Rev. 118 (1960) 1364.
- [28] J. Lowe et al., Phys. Rev. C44 (1991) 956.
- [29] A.A. Bel'kov et al., Sov. J. Nucl. Phys. 31 (1980) 96.
- [30] A.A. Bel'kov et al., Sov. J. Nucl. Phys. 28 (1978) 657.
- [31] S.A. Bunyatov et al., Sov. J. Nucl. Phys. 25 (1977) 177.
- [32] A.V. Kratsov et al., Sov. J. Nucl. Phys. 20 (1975) 500.
- [33] M.D. Manley, Phys.Rev. D30 (1984) 536.
- [34] R. Müller et al., Phys. Rev. C48 (1993) 981.
- [35] M.D. Manley, Phys.Rev. D30 (1984) 904.
- [36] U. Bohnert, Thesis, University of Erlangen, 1993.
- [37] D. Malz, Thesis, University of Erlangen, 1989.

Figures

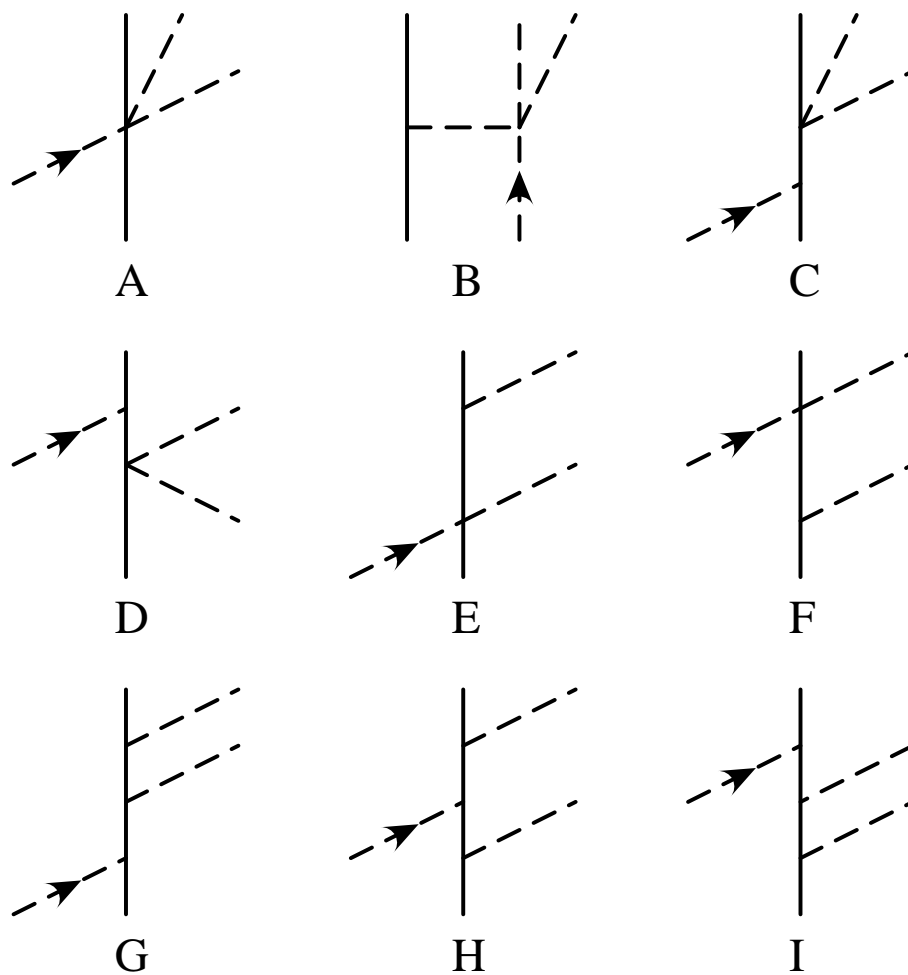


Figure 1: Tree graphs with insertions from the dimension one Lagrangian. The incoming pion is marked with an arrow. Diagrams with the final two pions exchanged ($b \leftrightarrow c$) are not shown.

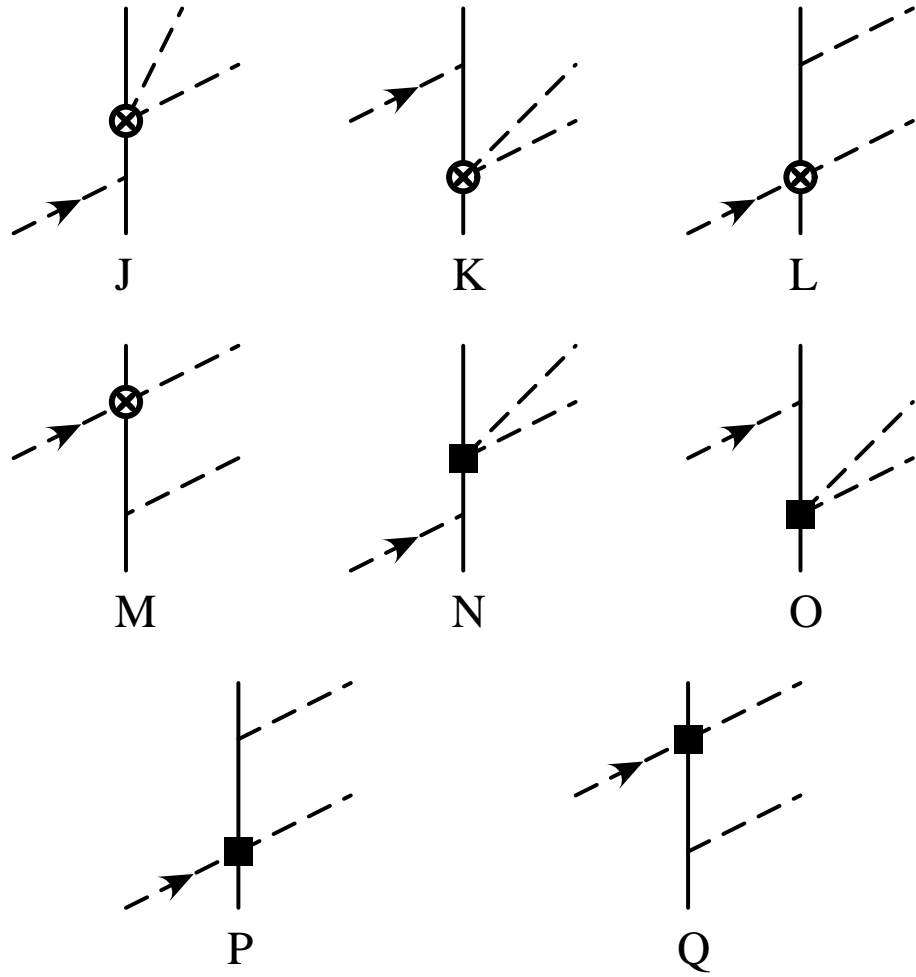


Figure 2: Tree graphs with exactly one insertion from the dimension two Lagrangian. The incoming pion is marked with an arrow. The circled cross and the box denotes an insertion proportional to c_1, c'_2, c''_2, c_3 and c_4 , respectively. Diagrams with the final two pions exchanged ($b \leftrightarrow c$) are not shown.

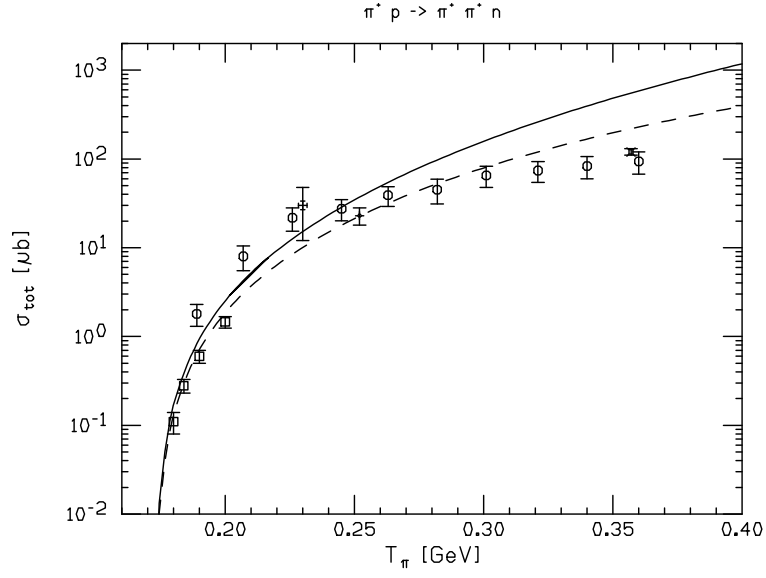


Figure 3: Total cross section for $\pi^+ p \rightarrow \pi^+ \pi^+ n$.

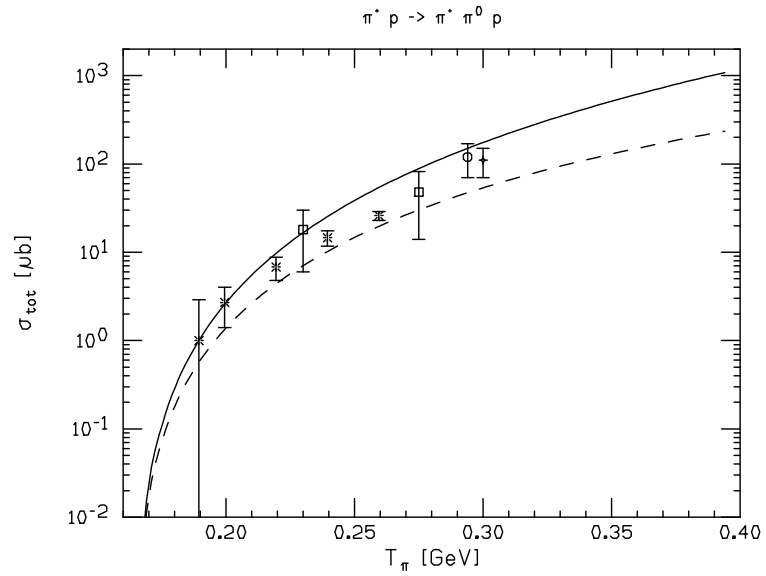


Figure 4: Total cross section for $\pi^+ p \rightarrow \pi^+ \pi^0 p$.

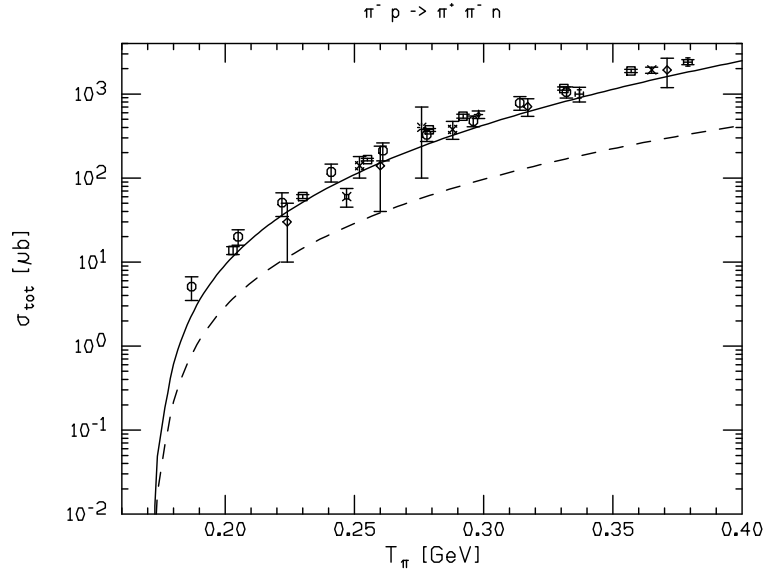


Figure 5: Total cross section for $\pi^- p \rightarrow \pi^+ \pi^- n$.

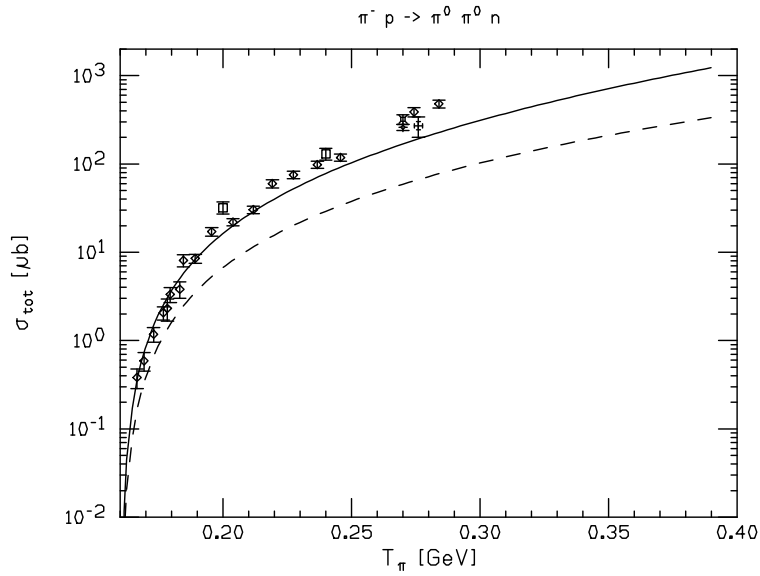


Figure 6: Total cross section for $\pi^- p \rightarrow \pi^0 \pi^0 n$.

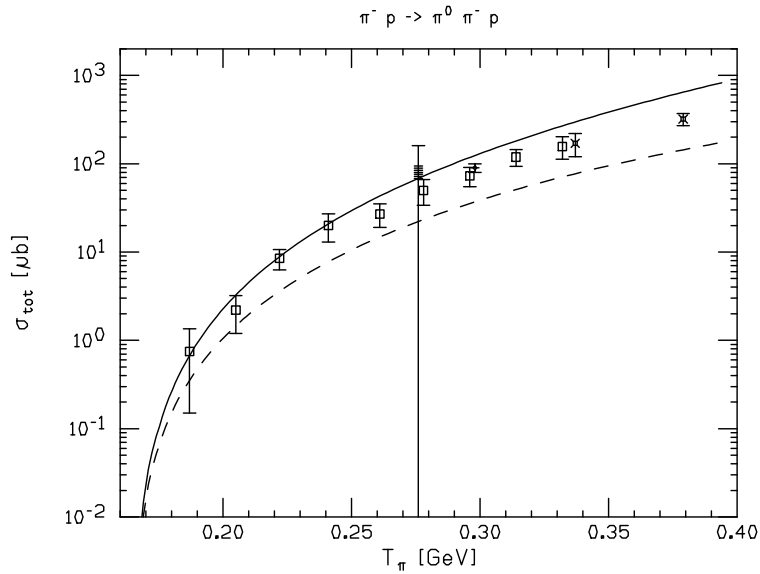


Figure 7: Total cross section for $\pi^- p \rightarrow \pi^0 \pi^- p$.

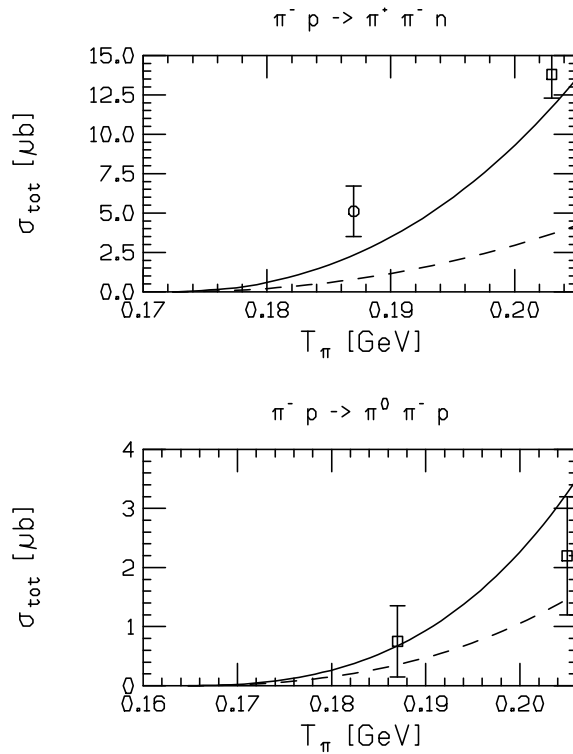


Figure 8: Threshold cross section for $\pi^- p \rightarrow \pi^+ \pi^- n$ and $\pi^- p \rightarrow \pi^0 \pi^- p$.

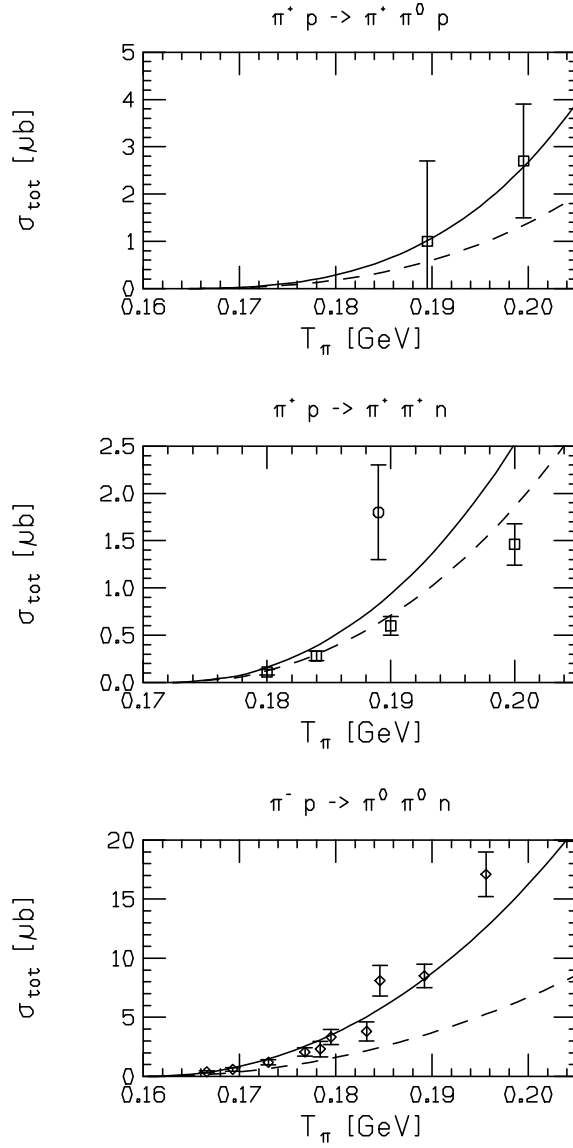


Figure 9: Threshold cross section for $\pi^+ p \rightarrow \pi^+ \pi^0 p$, $\pi^+ p \rightarrow \pi^+ \pi^+ n$ and $\pi^- p \rightarrow \pi^0 \pi^0 n$.

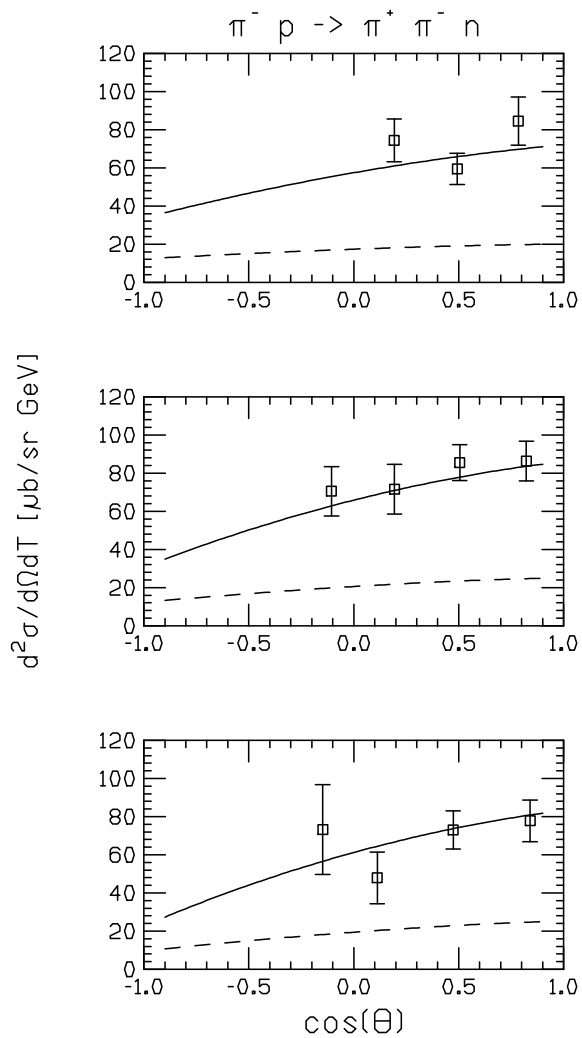


Figure 10: Double differential cross section at $\sqrt{s} = 1.242$ GeV in comparison to the data of [33] for $T_{\pi^+} = \omega_1 - M_\pi = 6.5, 10.95, 15.35$ MeV in the upper, middle and lower panel, respectively.

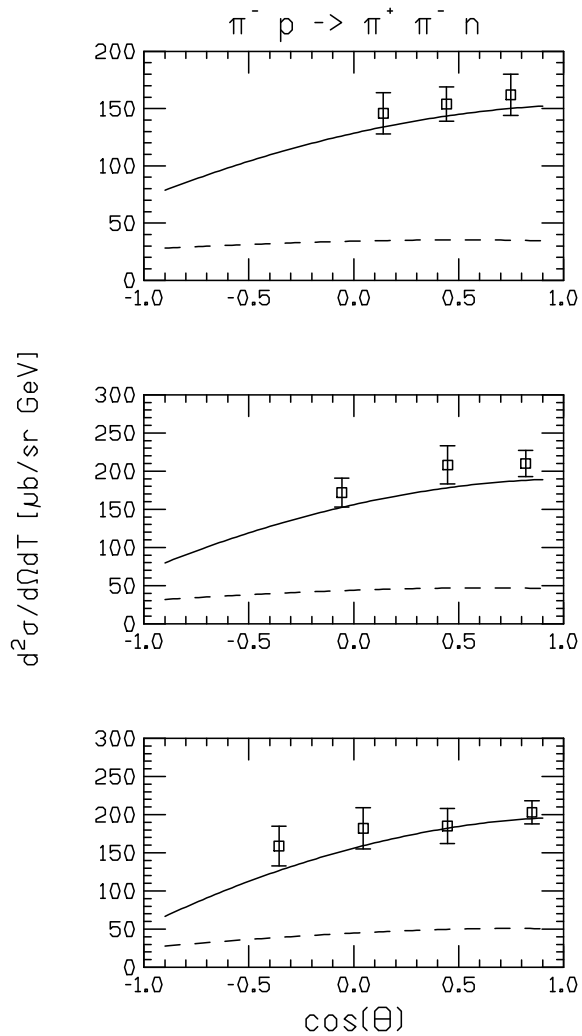


Figure 11: Double differential cross section at $\sqrt{s} = 1.262$ GeV in comparison to the data of [33] for $T_{\pi^+} = \omega_1 - M_\pi = 10.4, 17.5, 24.6$ MeV in the upper, middle and lower panel, respectively.

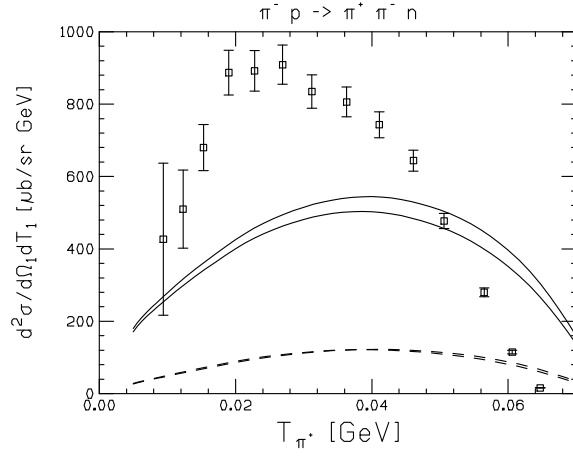


Figure 12: Double differential cross section for $\pi^- p \rightarrow \pi^+ \pi^- n$ in comparison to the data of [34] at $\sqrt{s} = 1.301$ GeV with $0.03 < x_1 < 0.35$. $T_{\pi^+} = \omega_1 - M_\pi$ is the kinetic energy of the emitted π^+ in the CMS.

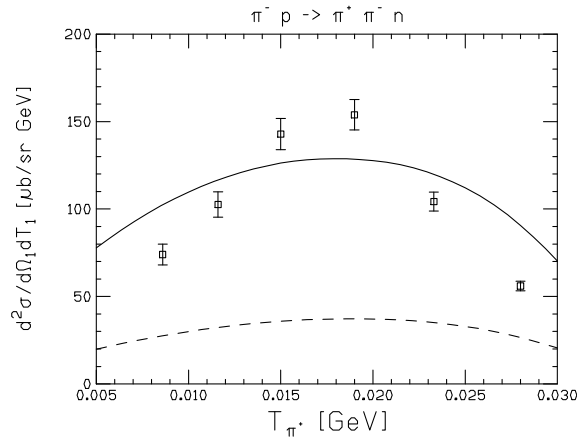


Figure 13: Double differential cross section for $\pi^- p \rightarrow \pi^+ \pi^- n$ in comparison to the data of [36] at the incoming pion energy $T_{\pi^-} = 218$ MeV at $x_1 = 0.19$. $T_{\pi^+} = \omega_1 - M_\pi$ is the kinetic energy of the emitted π^+ in the CMS.

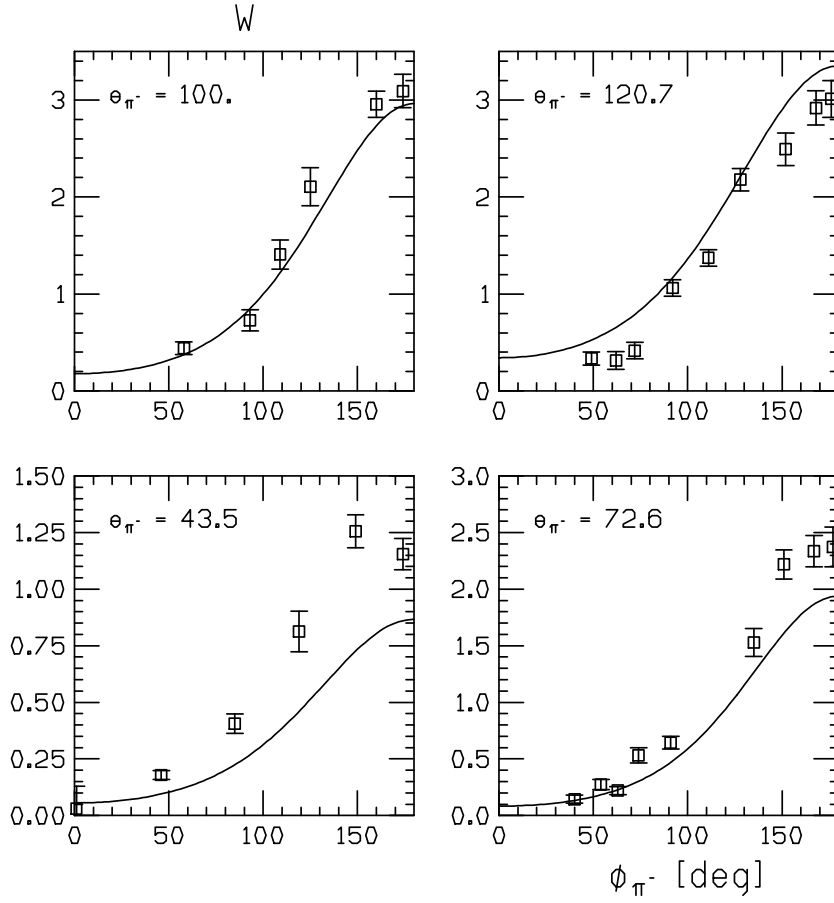


Figure 14: Angular correlation function W for $\pi^-p \rightarrow \pi^+\pi^-n$ in comparison to the data of [34] for the incoming pion energy $T_{\pi^-} = 284$ MeV at $|\vec{q}_1| = 127$ MeV and θ_2 as given in the various panels.

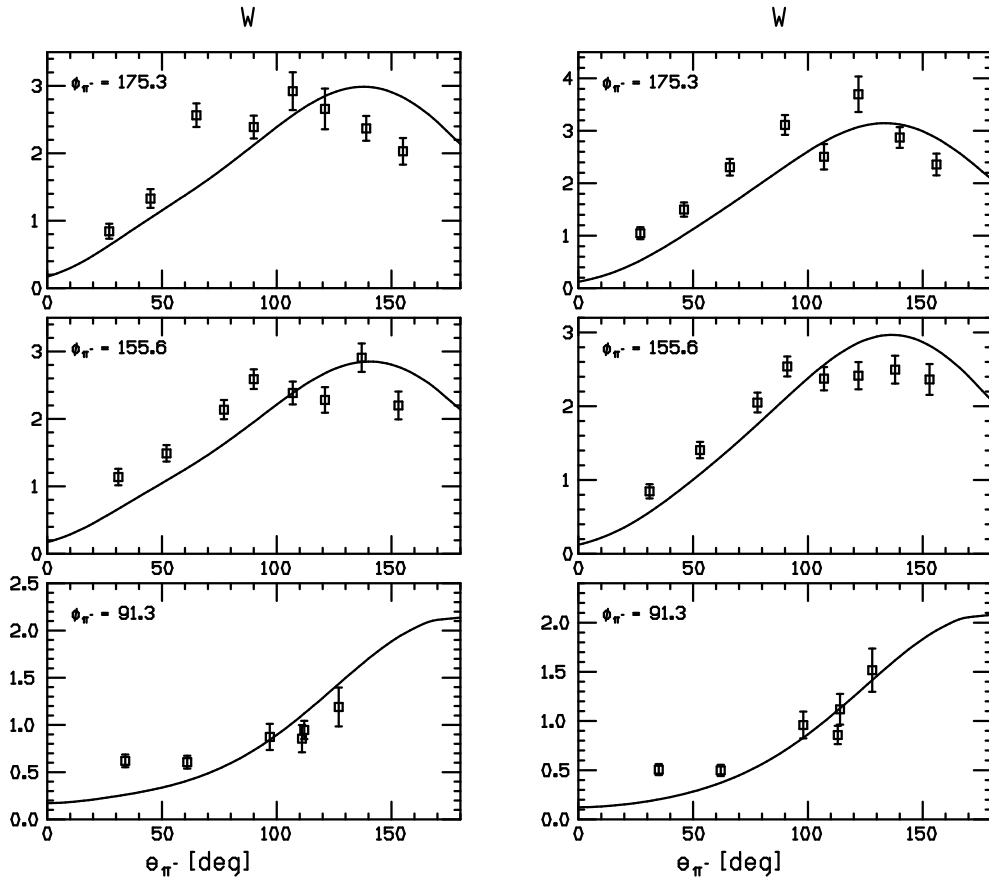


Figure 15: Angular correlation function W for $\pi^-p \rightarrow \pi^+\pi^-n$ in comparison to the data of [34] for the incoming pion energy $T_{\pi^-} = 284$ MeV at $|\vec{q}_1| = 60.5$ MeV and $|\vec{q}_1| = 86$ MeV (left and right panels, respectively) at fixed ϕ_2 as given in the various panels.